IEEE Photonics Journal
An IEEE Photonics Society Publication

Open Access

A 16 W Balanced Intensity Dual-Frequency Laser With 53 GHz Frequency Separation

Volume 8, Number 5, October 2016

Miao Hu
Mian Wei
Yu Zhang
Ju Cai
Ran Zeng
Qiliang Li

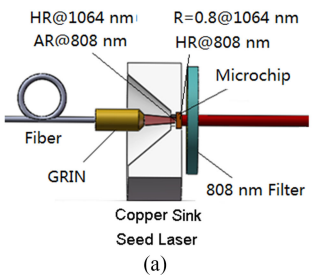

(a)

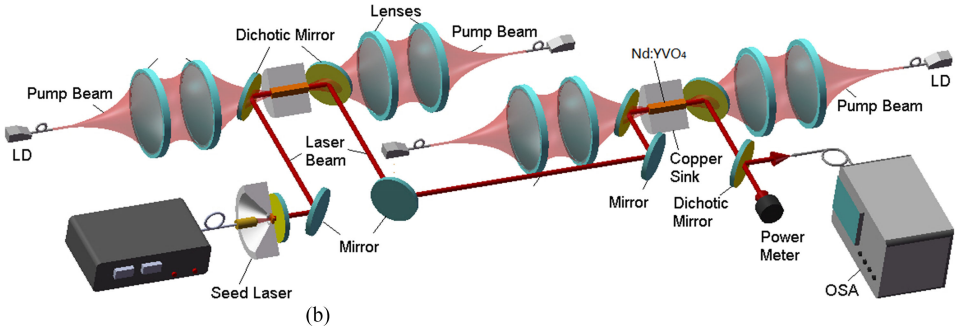

(b)

DOI: 10.1109/JPHOT.2016.2605456
1943-0655 © 2016 IEEE

A 16 W Balanced Intensity Dual-Frequency Laser With 53 GHz Frequency Separation

Miao Hu,[1] Mian Wei,[1] Yu Zhang,[1] Ju Cai,[2] Ran Zeng,[1] and Qiliang Li[1]

[1]College of Communication Engineering, Hangzhou Dianzi University, Hangzhou 310018, China.
[2]College of Communication Engineering, Chengdu University of Information Technology, Chengdu 610225, China.

DOI:10.1109/JPHOT.2016.2605456

Manuscript received July 27, 2016; revised August 25, 2016; accepted August 30, 2016. Date of publication September 2, 2016; date of current version September 19, 2016. The work was supported in part by the Open Foundation of State Key Laboratory of Advanced Optical Communication Systems and Networks under Grant 2015GZKF03008, in part by the Zhejiang Provincial Research Program of Public Welfare Technology Application under Grant 2016C31068, in part by the Natural Science Foundation of Zhejiang Province under Grant LY14A040008, and in part by the National Natural Science Foundation of China under Grant 11574068. Corresponding author: M. Hu (e-mail: miao_hu@foxmail.com).

Abstract: A 16.1 W continuous-wave balanced intensity dual-frequency laser based on an Nd: YVO_4 microchip seed laser, together with a two-stage laser amplifier, was demonstrated. In order to obtain such a high-power dual-frequency laser as well as a balanced intensity distribution of the dual-mode, the seed laser wavelength was precisely tuned to spectrally match with the gain curve of the amplifier by employing a temperature controller. Finally, when the heat sink temperature of the amplifier crystal was kept at 30.0 °C, the dual-mode seed laser operated at 16.0 °C was amplified from 284.5 mW to 16.1 W with a balanced intensity distribution, and frequency separation was measured as 53.2 GHz.

Index Terms: Microchip lasers, laser tuning, optical amplifiers

1. Introduction

Microwave photonics studies the generation, distribution, control, processing, and analysis of radio-frequency (RF) wave signals by means of photonics [1]. Recently, searching for high spectral purity photonic based RF wave signal sources becomes a compelling issue [2]–[4]. Among different methods of photonic RF wave generation technology, frequency beating based on dual-frequency diode-pumped solid-state lasers, provides an effective way for producing high spectral purity beat notes from the gigahertz (GHz) to even terahertz (THz) range [5], [6].

Over the past few years, several dual-frequency diode-pumped solid-state laser schemes have been proposed for the photonic RF wave signals generation. According to the emission cross-section (ECS) spectral shape of the gain materials, these dual-frequency lasers can be classified as three categories: 1) lasers based on the gain materials with dual-peak ECS spectral shape, e.g., c-cut Nd: $GdVO_4$ crystal and Nd: $LuVO_4$ crystal, etc. For instance, Wu obtained 4 W in σ polarization (1065.5 nm) and 1W in π polarization (1063.1 nm) dual-frequency laser with 0.63 THz frequency separation by use of Nd: $GdVO_4$ crystal [7]. Huang achieved 0.4 W in σ polarization (1085.7 nm) and 1.7 W in π polarization (1088.5 nm) dual-frequency laser with 0.71 THz frequency

separation by use of an Nd: $LuVO_4$ crystal [8]. These lasers offered high output power dual-frequency signals but with unbalanced intensity distribution of the dual-frequency component. 2) lasers based on the gain materials with wideband single-peak ECS spectral shape, e.g., Er: Yb: glass, Yb: $KGd(WO_4)_2$ and Ti: Sa crystals, etc., the ECS spectral bandwidths of which can exceed over 1 THz. For instance, Rolland realized a 7 mW dual-frequency laser with 0–1 THz tunable frequency separation based on a double-axis Er: Yb: glass laser, in which etalons and $LiNbO_3$ crystals were used for frequency separation tuning [9], [10]. Brenier reached the goal of a dual-frequency laser with frequency separation tuning range of 0–7.8 THz by exploying chirped bragg gratings in a Yb: $KGd(WO_4)_2$ laser [11]. Loas utilized two Ti: Sa crystals in a laser cavity and achieved 50 mW dual-frequency laser output with frequency separation between 0–1.5 THz [12]. These lasers offered dual-frequency laser signals with tunable frequency separation as well as balanced intensity distribution of the dual-frequency component. However, because of the small ECS values of such gain materials, the output power of such dual-frequency lasers was rather low. 3) lasers based on the gain materials with narrowband single-peak ECS spectral shape, e.g., Nd: YAG and Nd: YVO_4 crystal, whose ECS spectral bandwidths are 0.16 THz and 0.25 THz, respectively. For instance, McKay produced a 20 mW tunable dual-frequency laser signal with maximum frequency separation at 0.15 THz by using an Nd: YAG microchip laser [13]. Tani achieved an 860 mW dual-frequency laser signal with 0.1 THz frequency separation by using an Nd: YVO_4 microchip laser [14]. Yang applied the non-mode-locked scheme to a dual-longitudinal-mode Nd: YVO_4 microchip laser and realized 116 mW dual-frequency laser output with 0.1–0.2 THz tunable frequency separation [15]. These lasers also offered dual-frequency laser signals with tunable frequency separation as well as balanced intensity distribution of the dual-frequency component. However, due to the short gain media in length of such microchip lasers, the optical output power scale was limited. In order to fulfill the dual-frequency laser requirements of both high power output and balanced intensity distribution, a master oscillator power amplifier (MOPA) architecture with injection seeding of a dual-frequency master oscillator was recommended. Miao Hu proposed balanced intensity dual-frequency seed laser with a balanced gain single-stage amplifier, and achieved laser signal with frequency separation at 45.88 GHz and output power at 2.38 W [16]. However, their balanced gain amplification still limited the output power scale. In this paper, we proposed a dual-frequency laser with 16.1 W output power based on an unbalanced intensity dual-frequency seed laser with a complementary gain two-stage amplifier. We precisely tuned the temperature of the seed laser at a relative low temperature for higher output power and made a complementary gain between the two components of the seed laser and the amplifier. The seed laser mode with lower intensity received a higher amplification gain, while the higher intensity mode of the seed laser received a lower amplification gain, which was very different from the past research. The paper is organized as follows. In Section 2, the experimental setup of dual-frequency MOPA system is presented. In Section 3, the output power and optical spectra of both the seed laser and the amplified laser are then experimentally investigated. Conclusions are drawn in the last Section.

2. Layout of the Laser System

In order to obtain a high power dual-frequency laser as well as a balanced intensity distribution of the dual-frequency component, we had to employ a two-stage MOPA laser system with “spectral match” function. A precise temperature controller of the seed laser cavity was needed in the MOPA laser system for shifting the spectra of the seed laser signals, and matching with the gain curve of the amplifier. The experimental setup of the dual-frequency MOPA system was as follows. Fig. 1 shows the schematic of the dual-frequency MOPA laser system. The pump source of the seed laser was a fiber coupled laser diode (LD) operated at 808 nm, offering 5.0 W pump power maximum. Through a graded refractive index lens (GRIN, referred as self-focusing lens, or SOLFOC lens, Ø1.8 mm, 0.29 Pitch, uncoated), the pump light was delivered into the Nd: YVO_4 microchip crystal with spot radius of 0.2 mm and NA of 0.22. In order to realize stable dual-longitudinal-mode resonance of the seed laser, we had to make sure the cavity mode separation of the microchip laser was larger

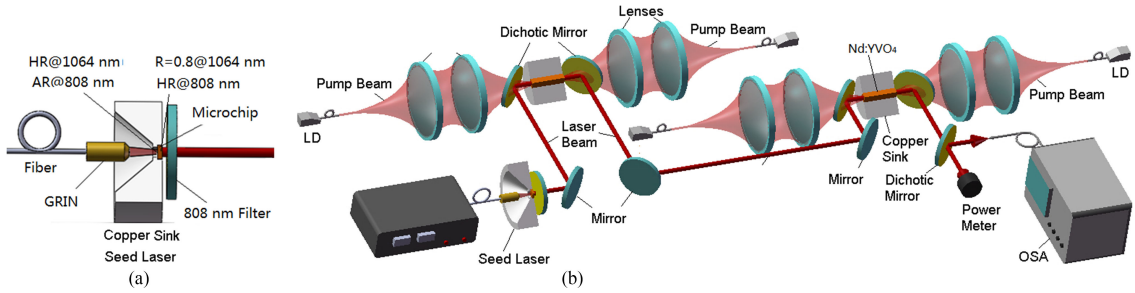

Fig. 1. (a) Schematic of the master oscillator seed laser and (b) "U" shape two-stage MOPA system. GRIN: Graded Refractive Index Lens. OSA: Optical Spectrum Analyzer.

than the half of the gain bandwidth of the gain medium and less than the entire gain bandwidth [16]. Therefore, the dimension of the monolithic microchip seed laser crystal was 3 mm $\times$ 3 mm $\times$ 1 mm (Castech Inc.), of which cavity mode separation was calculated about at 65 GHz. The Nd^{3+} concentration of microchip crystal was 1.0% and the absorption coefficient at pump wavelength was 31.3 cm-1. The input and output mirror were directly coated on the surface of the microchip crystal. The input mirror had a high reflectivity R $>$ 99.5%@1064 nm and high transmission T $>$ 80%@ 808 nm, the output mirror had a reflectivity of R $=$ 80%@1064 nm, and high reflectivity R $>$ 99.5%@ 808 nm. Here, the R $=$ 80% reflectivity of output mirror at 1064 nm was to make sure the seed laser operated at a low multiple of the threshold power and kept it with only two longitudinal modes. The seed laser was optically isolated from the two-stage amplifier to prevent lasing between the oscillator mirrors and the amplifier.

The generated dual-frequency seed laser was fed into the amplifier by mirrors and dichroic mirrors (DM). A Kepler telescope was introduced to realize good mode overlap between the seed laser beam and the gain area of the amplifier, further optimized the amplification efficiency and beam quality. The microchip crystal was wrapped with indium foil and mounted in a thermoelectric-cooled (TEC) heat sink for wide range precise temperature controlling. In the following paragraphs, the temperature of the seed laser heat sink was defined as T_c.

The employed power amplifier was a two-stage "U" shape double-end LD pumped traveling wave amplifier configuration. Both the Nd: YVO_4 crystals of amplifier had an Nd^{3+} doping concentration of 0.3% and a dimension of 3 mm $\times$ 3 mm $\times$ 12 mm. The comparatively long dimension in longitudinal direction and low Nd^{3+} doping concentration of the amplifier crystals brought a uniform gain distribution in amplification process, which facilitated a good management of the amplified laser beam quality. Through optical lenses systems and dichroic mirrors the pump lights were dual-side focused into the amplifier crystals and constructed a two-stage "U" shape scheme. Here, each pump light was fiber-coupled LD with the fiber diameter as 400 μm and Numerical aperture (NA) as 0.22. The dichroic mirrors were coated with a high reflectivity R $>$ 99.9%@1064 nm and a high transmission T $>$ 96%@808 nm. To avoid the temperature free-running state induced instability of the amplifier crystals gain curve, the amplifier crystals were also wrapped with indium foil and mounted in TEC based heat sinks. The temperature of the heat sinks was controlled by TECs at const. The output seed laser beam and amplified laser beam were split into two paths, respectively. On one path, the seed laser output power (PSL) and amplified laser output power (PAL) were measured by power meter (30A-BB-18, Ophir Inc.); on the other path, the lasers were fed into a high resolution (0.01 nm) OSA for spectral analysis (AQ 6319, Yokogawa Inc.).

3. System Output Data

3.1 Seed Laser Output

By maintaining the pump power of the seed laser (P_{LD}) at 1.7 W (it is unwise to raise the pump power over 4.0 W in our experiment setup because the high level pump power may lead to a large thermal

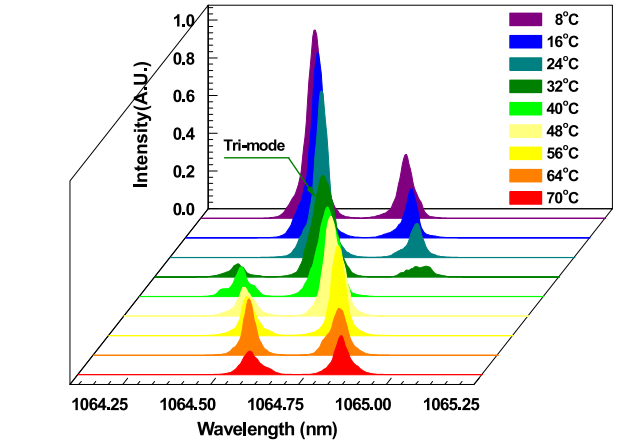

(a)

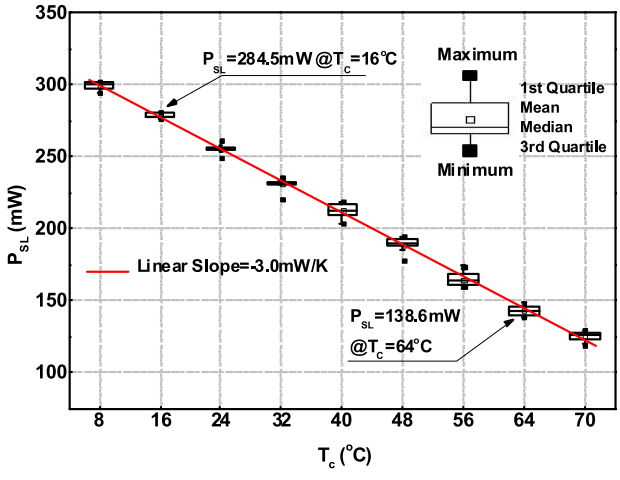

(b)

Fig. 2. Characteristics of the seed laser. (a) Red shift of seed laser spectral per 5 °C when tuning T_c from 8.0 °C to 70.0 °C. CWSL = central wavelength of seed laser. (b) Box chart of P_{SL} versus T_c when P_{LD} was fixed at 1.7 W, presenting a linear thermal-induced decrease.

gradient in microchip laser crystal and cause thermal induce fragmentation), we employed a water cooled TEC to control the temperature of the microchip crystal copper sink. Under the condition of fixed cavity length, the ECS spectrum of the microchip crystal as well as the wavelength of the seed laser red shift along with the increasing of T_c, which together determine the dual-mode wavelength location of the seed laser [17], as shown in Fig. 2(a).

As P_{LD} was set at 1.7 W, when T_c increased from 8.0 °C to 29.0 °C, the short-wavelength mode spectrum of the dual-frequency seed laser shifted from 1064.42 nm to 1064.57 nm; and the long-wavelength mode shifted from 1064.66 nm to 1064.81 nm. When T_c was at 30.0–33.0 °C, the dual-mode wavelengths location experienced a “mode hoping” and a temporary tri-mode resonance occurred in the cavity. When T_c increased from 34.0 °C to 70.0 °C, the short-wavelength mode shifted from 1064.35 nm to 1064.60 nm; and the long-wavelength mode shifted from 1064.60 nm to 1064.86 nm. During the dual-mode wavelengths shifting, the frequency separation remained stable around 65 GHz, corresponding to 0.24 nm at wavelength separation. The linear fit wavelength shift coefficients of the dual-mode were 6.25 pm/K (8.0–29.0 °C) and 6.66 pm/K (34.0–70.0 °C), respectively.

What interested us more was the amplitude variation of the dual-mode intensity as T_c increased, shown in Fig. 2(a). When T_c was between 8.0 °C to 29.0 °C, the short-wavelength mode intensity

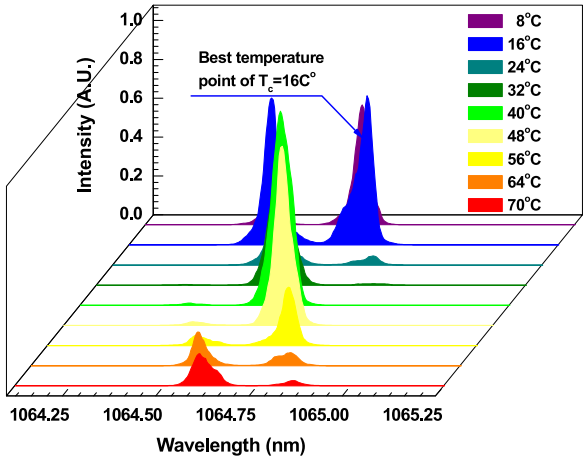

Fig. 3. Simulation of the amplification process when $T_c = 8.0$–$70.0\,^{\circ}$C, shown with normalized intensity. Intensity balanced dual-frequency amplified laser appeared at $T_c = 16.0\,^{\circ}$C. At $T_c = 64.0\,^{\circ}$C, the amplified laser output was neither intensity balanced distribution nor powerful, subject to the "spectral mismatch" and thermal induced power decrease.

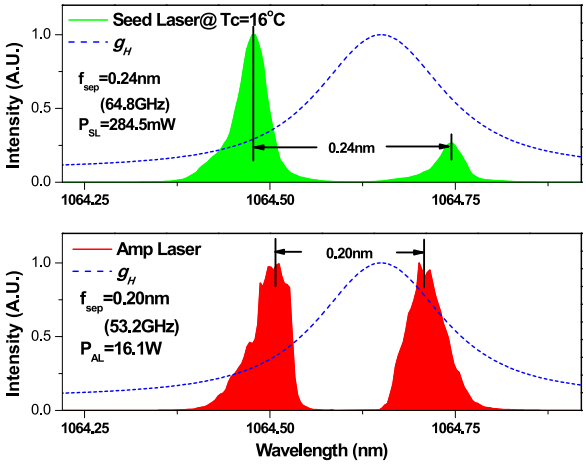

(a)

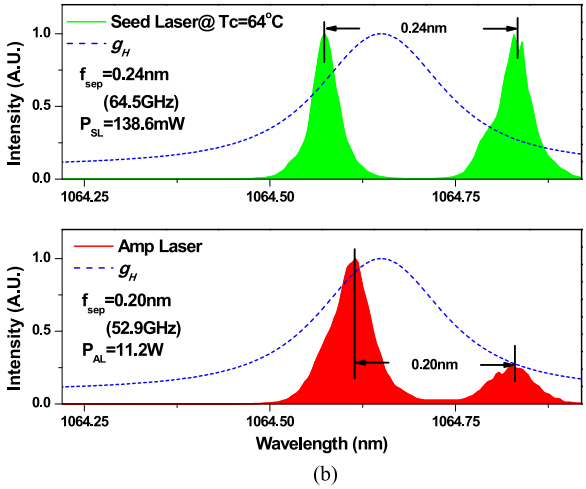

(b)

Fig. 4. Normalized spectra of seed laser and amplified laser. (a) $T_c = 16.0\,^{\circ}$C. (b)Tc $= 64.0\,^{\circ}$C. fsep = frequency separation. Dash-line: small signal gain curve of amplifiers.

was larger than the long-wavelength mode, which could be recognized as unbalanced intensity distribution of the dual-mode output. When T_c reached 30.0 °C, the "mode hopping" reversed the intensity distribution of the dual-mode, and the short-wavelength mode intensity began to fall while the long-wavelength mode intensity began to rise. When T_c continued to increase, the long-wavelength mode and the short-wavelength mode intensity began to draw equally. When T_c reached 64.0 °C, the dual-mode seed laser operated in a balanced intensity distribution with 138.6 mW output power.

Conceivably, the dual-mode intensity distribution variation was explained as caused by the different red-shift rate between the ECS spectrum and laser wavelengths with T_c increasing. Actually, the ECS spectrum center red-shift with T_c increasing was coincided with the central wavelength of the dual-mode spectral envelope but the laser wavelengths red-shift. Another phenomenon associated with T_c increasing was the output power reduction of the dual-frequency seed laser signal, which was caused by the reduction of the ECS value. Here, the output power of the seed laser was measured with a linear reduction as −3.0 mW/K, as shown in Fig. 2(b).

Generally, a balanced intensity dual-frequency laser facilitates good beat-note efficiency, however, according to Fig. 2, the output power of the balanced intensity seed laser was relatively small ($Tc \approx 64.0$ °C), which limited its further application in beat-note signal generation. A further power amplification of the seed laser with balanced intensity distribution output was highly needed.

For microchip seed laser, due to the relatively lower heat dissipation ability and higher Nd^{3+} doping concentration, the laser area temperature of the seed laser crystal was generally higher than the amplifier crystals, which led to an ECS spectrum gap between them. Considering the dual-mode seed laser spectral envelope center was coincided with the ECS spectral center of the microchip laser crystal, the center wavelength of the seed laser spectral envelope also presented a gap with the gain curve center of the amplifier crystals. As a result, a balanced intensity dual-mode seed laser would not receive equal gain, which led to unbalanced intensity amplification. In order to overcome the above drawback, here, we need to employ the "spectral match" mechanism in the amplification process. The "spectral match" mechanism means that the seed laser mode with lower intensity received a higher amplification gain, while the higher intensity mode of the seed laser received a lower amplification gain.

3.2 Amplified Laser Output

Here, we introduced the mathematical model of "spectral match" mechanism [18] in the traveling wave amplification process, and deduced the best temperature point of T_c for balanced intensity dual-frequency laser amplification. According to the principle of traveling wave laser amplification, we have

$$g_H(v, I) \sim \frac{1}{1 + I/I_{\text{sat}}} \cdot \frac{(\delta v/2)^2}{(v - v_0)^2 + (\delta v/2)^2} \tag{1}$$

$$\delta v = \sqrt{1 + I/I_{\text{sat}}} \times \Delta v_H . \tag{2}$$

Here, Δv_H is the ECS bandwidth of Nd: YVO_4 crystals in the amplifier, δ_v is the saturation broadened ECS bandwidth, and the ratio I/I_{sat} is dependent on the incident laser intensity I and the saturation intensity I_{sat}. The $g_H(v, I)$ is the gain coefficient dependent on frequency detune $(v - v_0)/\Delta v_H$ and the ratio I/I_{sat}, v_0 is the central frequency of the gain curve.

Since the ECS spectrum was highly dependent on the temperature of crystals, here, we set the temperature of amplifier crystals as const value (the temperature of amplifier crystal heat sink was controlled at 30 °C in experiments). The amplifier small signal gain curve was measured as center wavelength of 1064.65 nm and gain bandwidth of 0.22 nm. The seed laser mode which located near the gain curve center received higher gain than the other mode.

In our two-stage amplifier setup, the incident seed laser before the first-stage amplifier can be treated as a small signal. After the first-stage amplification, the intensity of the seed laser before the second-stage amplifier became comparable to the saturation intensity. In the second-stage

amplifier, when the stronger mode intensity of the seed laser gradually approached the saturation intensity value, the gain coefficient g_H decreased and the profile of the gain curve flatted, as showed in (2). This tendency was defined as saturation broadening or power broadening. After the saturation broadening, the dual-mode of the seed laser both shared less gain and the gain curve processed a wider spectral full-width at half-maximum (FWHM).

We took the seed laser case of $T_c = 8.0$–$70.0\,^{\circ}C$ into simulation, Fig. 3 illustrated the simulation results per 8.0 °C. In the case of $T_c = 64.0\,^{\circ}C$, after amplification, the balanced intensity dual-mode seed laser ($P_{SL} = 138.6$ mW) was amplified as an unbalanced intensity dual-mode laser. Because the long-wavelength mode of seed laser located farther away from the gain curve center rather than the short-wavelength mode, which was not fully amplified. In the case of $T_c = 16.0\,^{\circ}C$, with the unbalanced intensity dual-mode seed laser ($P_{SL} = 284.5$ mW), the dual-frequency amplified laser with balanced intensity distribution was achieved. The lower intensity long-wavelength mode of the seed laser had been amplified to the scale close to the stronger short-wavelength mode. The process from an unbalanced intensity distribution seed laser to a balanced intensity dual-mode amplified laser illustrated the dual-mode did not share equal gain in amplification but a complementary gain; we call this the "spectral match" amplification mechanism.

According to the anticipation simulated by the above model, we designed our experimental steps as follows: the seed laser beam was focused into the two-stage MOPA system. With temperature feedback control of both the seed laser and the amplifier, the pump power of the seed laser was kept at 1.7 W and the temperature T_c varied from 8.0–70.0 °C; the pump power of the amplifiers was kept at 20.0 W and the temperature of the amplifier crystals was kept at 30.0 °C. Based on the simulation results we set T_c at 16.0 °C and 64.0 °C, and re-examined the amplification process.

The experiment results almost repeated the simulation results, when T_c was set at 64.0 °C ($P_{SL} = 138.6$ mW), the amplified laser presented an unbalanced intensity dual-frequency component and the intensity ratio was 0.32. The total output power of amplified dual-frequency laser was 11.2 W, and the frequency separation $f_{sep} = 52.9$ GHz. When T_c was set at 16.0 °C ($P_{SL} = 284.5$ mW), the amplified laser with a balanced intensity distribution of the dual-frequency component was obtained, the intensity ratio was 0.98. The amplified dual-frequency laser output power P_{AL} was 16.1 W and the frequency separation $f_{sep} = 53.2$ GHz. Though noises emerged in the amplified laser, the goal of balanced intensity dual-mode had been realized.

The normalized experimental spectra of the seed laser and the amplified laser were shown in Fig. 4(a) and (b). The red pattern of amplified laser spectra of both Fig. 4(a) and (b) illustrates a tendency of frequency separation decrease. This phenomenon can be explained by the finite bandwidth of the amplifier gain curve. With a finite amplifier bandwidth, each mode of the seed laser in the amplification did not receive a flat-gain; therefore, the spectra of the amplified mode always tend to shift to the gain curve center; the tendency of this shift was in positive correlation with the amplifying magnitude.

4. Conclusion

A continuous-wave dual-frequency Nd : YVO_4 laser with large frequency separation and high output power was demonstrated experimentally. A microchip laser played a role as a master oscillator to produce dual-frequency seed laser signal. By means of a two-stage amplifier system and tuning temperature of microchip laser for "spectral match," the seed laser was amplified to 16.1 W with frequency separation up to 53.2 GHz. Such a high power output of dual-frequency laser is capable of serving as the optical source that can easily beat note signals with high frequency and low phase noise.

References

[1] R. Won, "Microwave photonics shines," *Nature Photon.*, vol. 5, 2011, Art. no. 736.
[2] S. Daryoosh and S. Safavi-Naeini, "Terahertz Photonics: Optoelectronic techniques for generation and detection of terahertz waves," *J. Lightw. Technol.*, vol. 26, no. 15, pp. 2409–2423, Aug. 2008.

[3] S Koenig *et al.*, "Wireless sub-THz communication system with high data rate," *Nature Photon.*, vol. 7, no. 12, pp. 977–981, 2013.
[4] A. J. Seeds *et al.*, "TeraHertz photonics for wireless communications," *J. Lightw. Technol.*, vol. 33, no. 3, pp. 579–587, Feb. 2015.
[5] O. Kyoung-Hwan *et al.*, "High-sweeping-speed optically synchronized dual-channel terahertz-signal generator for driving a superconducting tunneling mixer and its application to active gas sensing," *Opt. Exp.*, vol. 17, no. 21, pp. 18455–1846, 2009.
[6] A. R. Criado *et al.*, "Observation of phase noise reduction in photonically syntesized sub-THz signals using a passively mode-locked laser diode and highly selective optical filtering," *Opt. Exp.*, vol. 20, no. 2, pp. 1253–1260, 2012.
[7] B. Wu *et al.*, "Compact dual-wavelength Nd: $GdVO_4$ laser working at 1063 and 1065 nm," *Opt. Exp.*, vol. 17, no. 8, pp. 6004–6009, 2009.
[8] Y. P. Huang *et al.*, "Orthogonally polarized dual-wavelength Nd: $LuVO_4$ laser at 1086 nm and 1089 nm," *Opt. Exp.*, vol. 20, no. 5, pp. 5644–5651, 2012.
[9] A. Rolland *et al.*, "Narrow linewidth tunable terahertz radiation by photomixing without servo-locking," *IEEE Trans. Terahertz Sci. Technol.*, vol. 4, no. 2, pp. 260–266, Mar. 2014.
[10] G. Danion *et al.*, "Dual frequency laser with two continuously and widely tunable frequencies for optical referencing of GHz to THz beatnotes," *Opt. Exp.*, vol. 22, no. 15, pp. 17673–17678, 2014.
[11] A. Brenier, "Tunable THz frequency difference from a diode-pumped dual-wavelength Yb^{3+}: $KGd(WO_4)_2$ laser with chirped volume Bragg gratings," *Laser Phys. Lett.*, vol. 8, no. 7, pp. 520–524, 2011.
[12] G. Loas *et al.*, "Dual-frequency 780-nm Ti: Sa laser for high spectral purity tunable CW THz generation," *IEEE Photon. Technol. Lett.*, vol. 26, no. 15, pp. 1518–1521, Aug. 2014.
[13] A. Mckay and J. M. Dawes, "Tunable terahertz signals using a helicoidally polarized ceramic microchip laser," *IEEE Photon. Technol. Lett.*, vol. 21, no. 7, pp. 480–482, Apr. 2009.
[14] M. Tani *et al.*, "Generation of terahertz radiation by photomixing with dual- and multiple-mode lasers," *Semicond. Sci. Technol.*, vol. 20, no. 7, pp. S151–S163, 2005.
[15] Q Yang *et al.*, "Double-longitudinal-mode continuous-wave laser with ultra-large frequency difference used in narrowband terahertz wave generatio," *Acta Optica Sinica*, vol. 33, no. 5, pp. 154–160, 2013.
[16] Miao Hu *et al.*, "CW dual-frequency MOPA laser with frequency separation of 45 GHz," *Opt. Exp.*, vol. 23, no. 8, pp. 9881–9889, 2015.
[17] D. Xavier, F. Balembois, and P. Georges, "Temperature dependence of the emission cross section of Nd: YVO_4 around 1064 nm and consequences on laser operation," *J. Opt. Soc. Amer. B*, vol. 28, no. 5, pp. 972–976, 2011.
[18] A. E. Siegman, *Lasers*. Sausalito, CA, USA: University Science, 1986, pp. 862–863,